ELECTRONIC PROPERTIES OF STOICHIOMETRIC TITANIUM ALLOY CRYSTALS: II, SUSCEPTIBILITY OF BODY-CENTERED CUBIC TITANIUM

R. A. Tawil

Department of Physics, University of Petroleum and Minerals, Dhahran, Saudi Arabia

الخلاصة

سجلت نتائج الحسابات المتوافقة والمعدلة بشكل محكم في بناء الطرق للتيتانيوم التكعيبي وتستخدم هذه النتائج لحساب حساسية الالكترون الموصل الغير متفاعل لهذا الكريستال .

ان الكثافة الكبيرة للحالات في مستوى (Fermi) وتداخل سطح (Fermi) وحدوث الذروة في الحساسية قد استخدمت جميعا في مناقشة الكفاية وذلك بهدف التحقق من عدم الاستقرار الشبكى الحاصل في هذا الطور للتيتانيوم .

ABSTRACT

Results of a self-consistent modified tight-binding calculation of the bandstructure of body-centered cubic titanium are reported. These results are discussed, and used to calculate the noninteracting conduction electron susceptibility for this crystal. The large density of states at the Fermi level, the nesting of the Fermi surface, and the occurrence of peaks in the susceptibility were used, in a sufficiency argument, to investigate the lattice instability occurring in this phase of titanium.

0377-9211/79/0104-0019$01.00

ELECTRONIC PROPERTIES OF STOICHIOMETRIC TITANIUM ALLOY CRYSTALS: II, SUSCEPTIBILITY OF BODY-CENTERED CUBIC TITANIUM

1. INTRODUCTION

The energy-band method is a successful scheme for obtaining accurate and readily usable eigensolutions of the effective one-electron Hamiltonian, and has been applied to a large number of real systems. Based on the eigenvalues, physical properties such as the density of states (DOS), Fermi surface topology [1], and response functions [2] have been calculated. The eigenfunctions have been used in the calculations of the X-ray form factors, Compton profiles [3], positron annihilation, and the optical properties [4, 5] of a variety of metallic and semiconducting crystals. These calculated physical quantities are found to be in good agreement with experimental ones [6]. Further, the eigensolutions have also been used to study electronically driven instabilities in metals [7–9]. These instabilities, as formulated by Kubo *et al.* [10] and recently reviewed by Chan and Heine [11], are thought to result from a divergence in the generalized static electronic susceptibility, $\chi(\mathbf{q})$.

This paper reports on the bandstructure of body-centered cubic (BCC) titanium, and the resulting calculation of $\chi(\mathbf{q})$ for this metal is presented. The structure obtained in the $\chi(\mathbf{q})$ is then used in an attempt to account for the instability of the BCC crystal phase of titanium.

Two forms of titanium are known. α-Ti, stable at room temperature, has a close packed hexagonal structure with $a = 2.950$ Å, $c = 4.683$ Å, and $c/a = 1.587$. The electronic structure [12–14], Fermi surface topology [15, 16], and the possibility of the occurrence of magnetic breakdown [17] are some of the physical properties investigated for this phase. Three of the findings that are relevant to the thesis of this paper will be singled out: (i) The DOS at the Fermi level is found to be close to 22.0 electrons/atom/Rydberg [12, 13]; (ii) No Fermi surface nesting (existence of large parallel pieces) has been reported [12–14]; and (iii) The de-Haas–van Alphen measurements indicate that the Fermi surfaces of Ti and Zr are quite similar [15, 16].

The other form is β-Ti which has the body-centered cubic structure. This phase cannot be retained by quenching pure Ti. It is unstable at room temperature, undergoing a transition to the α-phase at about 882°C [18]. However, as shown in Figure 1 [19], the β-phase can be retained at room temperature by quenching Ti in alloys containing at least 5 atomic % solute of Mn, Fe, and V. There is another important feature to the figure. The various quenched alloys, when extrapolated to zero solute content, predict that the lattice spacing of β-Ti at room temperature is 3.295 Å. The scatter about this value of the lattice constant is reported [18] to be 0.2%. If one regards the progressive decrease in the atomic percentage of the solute as a lattice deformation of the β-phase of the Ti rich alloy, then a transition from the β- to the α-phase may be effected by the existence of a charge density wave [10, 11]. The mechanism and the necessary conditions for the existence of this process are elaborated in the rest of this section.

The reduction of the atomic percentage of a solute may be regarded as a spatially inhomogeneous perturbation. It involves a rearrangement of the positive ions. This deformation has the effect of promoting conduction electrons from an originally occupied region of the reciprocal space (k-space) to populate an unoccupied one. If the redistribution is such that the electrons are scattered from orbitals with no spin flip, the instability is of the nature of lattice distortion coupled to a charge density wave. If it involves a spin flip then the instability manifests itself as a spin density wave [20].

To first order, the response of the electrons to such perturbations is measured by the generalized static susceptibility with Fourier components:

$$\chi^{(0)}(\mathbf{q}) = \frac{\chi(\mathbf{q})}{1 - I(q)\chi(\mathbf{q})} \tag{1}$$

Here $I(\mathbf{q})$ denotes the electron–electron interaction term, and $\chi(\mathbf{q})$ is given in the random phase approximately by

$$\chi(\mathbf{q}) = \sum_{\substack{n,m \\ \mathbf{k}}} |M_{n,m}(\mathbf{k}+\mathbf{q},\mathbf{k})|^2 \frac{f(E_n(\mathbf{k}))[1 - f(E_m(\mathbf{k}+\mathbf{q}))]}{E_m(\mathbf{k}+\mathbf{q}) - E_n(\mathbf{k})}, \tag{2}$$

where $E_n(\mathbf{k})$ is the energy of the Bloch electron at the point $\mathbf{k}$ of the Brillouin zone and in band n. The Fermi function $f(E_n(\mathbf{k}))$, at $T = 0$, has the value 0 or

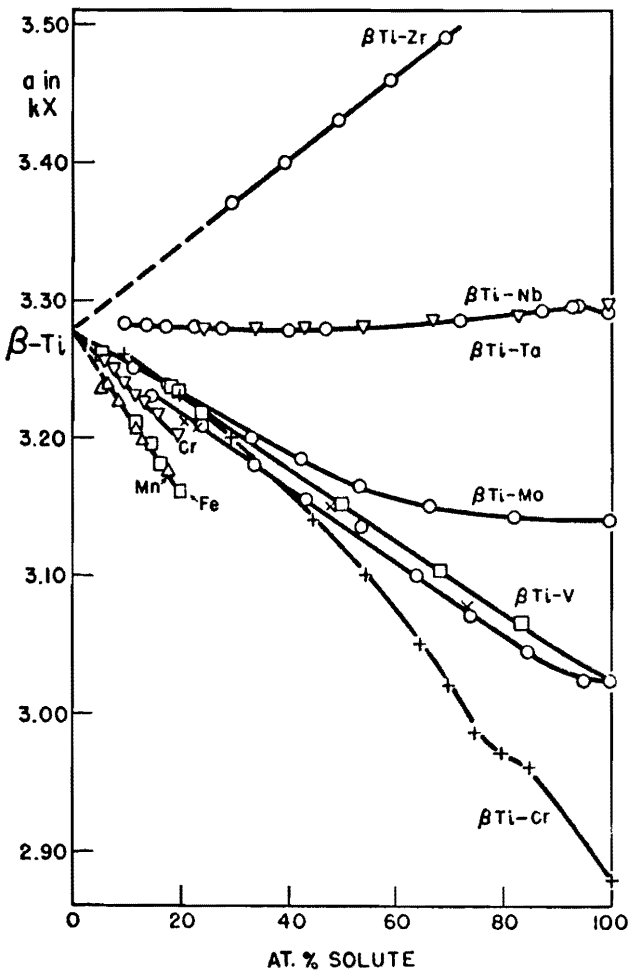

Ti–Cr + Cuff, Grant and Fior (1952).
Δ Duwez and Taylor (1952).
Ti–Fe □ Worner (1951).
Ti–Mn □ Maykuth, Ogden, and Jaffee (1953).
Ti-Mo ○ Hansen *et al.* (1951).
Ti–Nb □ Hansen *et al.* (1951).
Ti–Ta ○ Summers-Smith (1952).
Ti–V × Adenstedt, Piquignot, and Raymer (1952).
□ Powers and Wilhelm (1952).
○ Pietrokowsky and Duwez (1952).
Ti–Zr ○ Duwez (1952).

For further explanation of figure entries see References [18] and [19]

Figure 1. β-Titanium Solid Solution Lattice Spacings

1 depending on whether $E_n(\mathbf{k})$ is above or below the Fermi energy, E_F, respectively. $M_{n,m}$ is the oscillator strength matrix element and will be considered constant in this calculation. The constant matrix element approximation has been adopted by many researchers [7,8,21,22] and was found to be most valid for the interband transitions.

$\chi(\mathbf{q})$ is the 'bare' or noninteracting conduction electron susceptibility. This quantity, in linear response theory, gives the response of the magnetization of the electron gas in a metal to a spatially varying field of wave vector $\mathbf{q}$. An instability, of the type discussed earlier, sets in when this quantity diverges. The divergence happens in a nesting situation, that is, in a situation in which there are large areas of the Fermi surface which are parallel or nearly parallel.

Based on this model, several calculations have been performed [7,8,11,21,22] which made use of the $\chi(\mathbf{q})$ structure coupled to the phonon soft modes of the BCC structure to account for structural instabilities in Sc, Zr, and many of the rare-earth crystals. This same model is used here to investigate the instability of the β-Ti phase.

In Section 2 we present the energy-band model adopted, and discuss the resulting energy bands, density of states, and the Fermi surface topology for the body-centered cubic titanium. In Section 3 we display the Analytical Tetrahedron Linear Energy Method which makes use of the bandstructure results in order to calculate $\chi(\mathbf{q})$. The calculated susceptibility is presented and analyzed in the last section.

2. BANDSTRUCTURE

The present calculation was undertaken primarily in order to investigate the $\chi(\mathbf{q})$ for BCC titanium. Such an investigation requires us to generate accurate energy bands, density of states, and the Fermi surface for this metal.

Our calculation of the eigensolutions is self-consistent and parallels a recently reported calculation of the energy bands for face-centered cubic titanium [23]. The reader is referred to this paper for additional details concerning the method. In the present method we have used the Kohn–Sham–Gaspar local exchange potential [24]. No muffin-tin approximation is involved in this calculation.

The Bloch functions are constructed from a basis of independent Gaussian functions (IGF). The basis consists of 13 IGF for s symmetry, ten IGF for the radial part of each p symmetry, and five for the radial part of each d symmetry. In selecting the exponents we made use of the self-consistent calculation of the free titanium atom performed by Wachters [25]. The lattice constant is taken to be 3.295 Å.

The calculation was begun by constructing a crystal potential from a superposition of overlapping neutral-

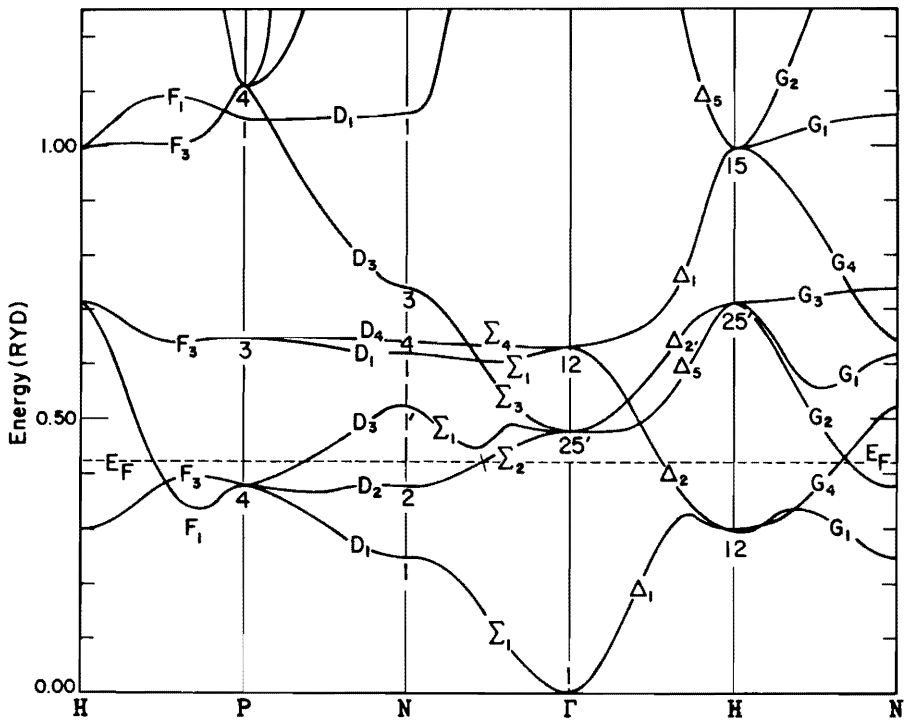

Figure 2. Energy Bands in BCC Titanium Along some Lines of High Symmetry. Lattice Constant Equals 3.295 Å

atom charge densities, the atom was assumed to be in the $3d^3 4s^1$ configuration. Energy levels and wave functions at 140 points in $\frac{1}{48}$th of the Brillouin zone were determined for this potential and used to initiate an iterative procedure leading to self-consistency. The iterative process was stopped when the change in the potential in two consecutive iterations was less than 1 part in 10^4.

The self-consistent eigensolutions are then used to trace the bandstructure, calculate the density of states, and map the orbits of the Fermi surface in the three crystallographic directions. The results are reported here.

Table 1. Selected Energy Levels of Electrons in Titanium. Energies are in Rydbergs

Γ_1	0.0000	N_1	0.2407
$\Gamma_{25'}$	0.4689	N_2	0.3717
Γ_{12}	0.6215	N_1'	0.5160
		N_1	0.6107
H_{12}	0.2908	N_4	0.6378
$H_{25'}$	0.7048	N_3	0.7310
H_{15}	0.9864		
P_4	0.3697	E_F = 0.4125	
P_3	0.6415		

2.1. Energy Bands

The calculated bandstructure along several high symmetry directions is presented in Figure 2. The bands show the expected hybridization between a narrow-d-band complex and a broad-s–p-band. Selected energies at high symmetry points are given in Table 1, and a comparison for some characteristic energy differences with the calculation of Snow and Waber [26] is effected in Table 2.

Table 2. Characteristic Energy-level Separations. Energies are in Rydbergs

	Present Calculation	Snow and Waber [26] Calculation
$H_{12}-\Gamma_1$	0.2908	0.27
$\Gamma_{25'}-\Gamma_1$	0.7048	0.52
$\Gamma_{25'}-H_{12}$	0.1781	0.26
$H_{25'}-H_{12}$	0.4140	0.44
N_1-N_4	0.3971	—

The calculation of Snow and Waber is an Augmented-Plane-Wave (APW) nonself-consistent calculation of

energy bands for all the 3d transition metals from scandium to copper. The calculation uses the unmodified Slater exchange and is aimed at determining which of the two atomic configurations, $4s^2\ 3d^n$ or $4s^1\ 3d^{n+1}$ is the favored in crystalline form. It was found to be the $4s^1\ 3d^{n+1}$.

The agreement between the two calculations is very poor. The starting potential in the two calculations is the same and this poor agreement may be attributed to self-consistent effects [27]. The self-consistency tends to broaden the d-band complex through s–d and p–d hybridizations and leaves the s–p band relatively unchanged.

2.2. Density of States

The density of states for this bandstructure is displayed in Figure 3. The two peaks at 0.36 Ry and 0.64 Ry are characteristic of all BCC structures and in this particular case arise from the nearly flat bands $H_{12} \leftrightarrow F_3 \leftrightarrow D_2 \leftrightarrow \Sigma_2 \leftrightarrow G_1$, and $H_{25}, \leftrightarrow F_3 \leftrightarrow D_1$ and $D_4 \leftrightarrow \Sigma_1$ and Σ_4' respectively. The Fermi level (E_F) is at 0.4150 Ry with respect to this origin, and the occupied portion of the d-band complex is 0.165 Ry. The total d-band width is 0.4140 Ry. The calculation of Snow and Waber gave a total width of 0.34 Ry, and an E_F lying in the same relative region of the first peak. The density of states at E_F is calculated to be 21.18 states/(Ry.-atom) as compared to the value of 22 obtained in Reference [26]. Our calculation yields an electron-specific-heat coefficient of 3.67 mJ mol^{-1} K^{-2}. The experimental value for this coefficient is 3.32 in the α-phase.

2.3. Fermi Surface

We have studied the Fermi surface which results from our calculation. It consists (i) a large electron surface about H. This surface supports an octahedral closed orbit in the (100) plane with distortions in the $H \rightarrow N$ and $H \rightarrow \Gamma$ directions. This surface does not support any closed orbits in the (110) or (111) planes; (ii) an electron surface that resembles a dumbbell around P and does not intersect the (110) and (111) planes; (iii) an ellipsoidal electron surface about N. This surface supports a closed orbit in the (100) plane, and in the (111) plane passing through H; (iv) a large electron hole about Γ. This hole is multiply connected in the (100) plane, and its intersection with the (110) plane results in a distorted circular orbit. The intersections of this electron hole with the (111) plane about Γ and H form octahedral orbits.

Surfaces enumerated (i) and (ii) result from the second band intersections with the Fermi level, and the other two result from the third band intersections. The cross sections of this Fermi surface in the (100), (110), and (111) planes are shown in Figures 4, 5 and 6, respectively. The dimensions of closed orbits for this surface are reported in Table 3.

From this table it can be observed that the dimensions of the intersections are clustered about the values of 0.45, and 0.55. Also, a careful survey of Figures 4–6 reveals that large segments of the electron hole about Γ (surface (iv)) in the (110) and (111) planes are parallel. It is clear that this Fermi surface is nested, and that the calculated susceptibility, $\chi(\mathbf{q})$, should

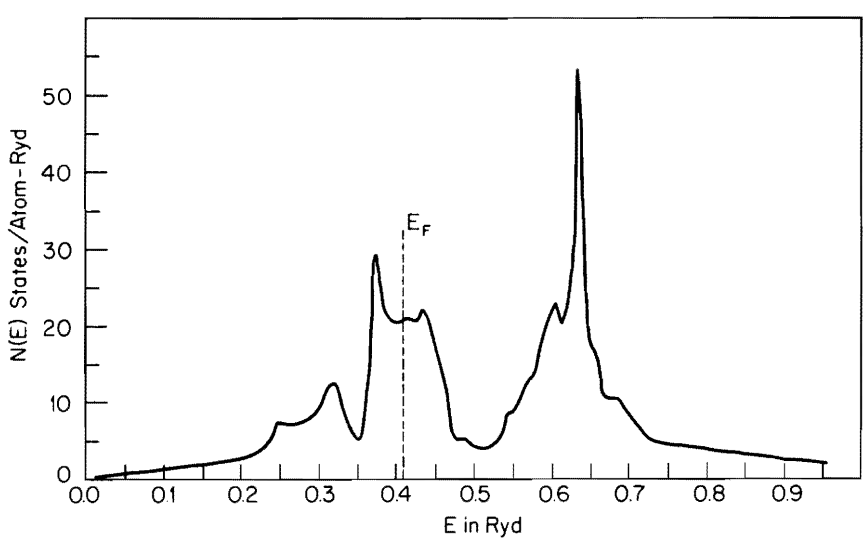

Figure 3: Density of States for BCC Titanium. The Density of States at the Fermi Level E_F is 21.18 States/atom-Ry

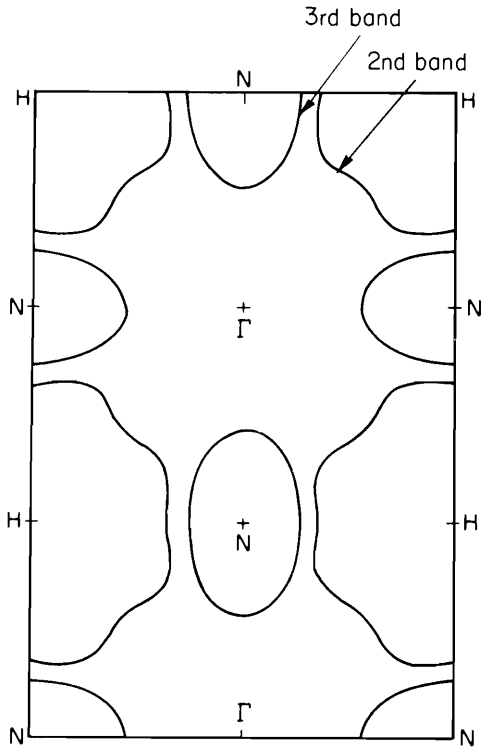

Figure 4. Fermi Surface Cross Sections in the (100) Planes

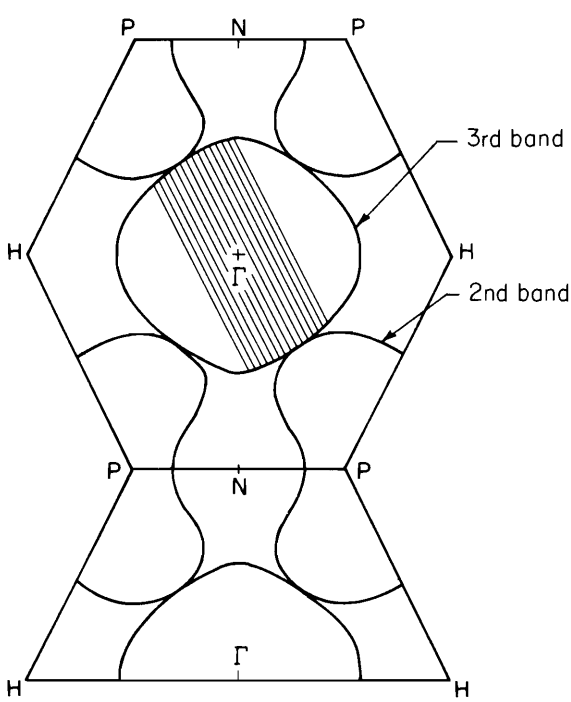

Figure 5. Fermi Surface Cross Sections in the (110) Plane

exhibit structures (peaks) at $|\mathbf{q}|$ values of 0.45 and 0.55 in units of $(2\pi/a)$.

3. CALCULATION OF THE SUSCEPTIBILITY

The calculation of the susceptibility of titanium that utilizes the bandstructure results presented in the previous section uses the Analytical Tetrahedron Linear Energy Method [7]. The irreducible part of the Brillouin zone, for which the $E_n(\mathbf{k})$ are calculated, is divided into nonoverlapping tetrahedra. Each of these tetrahedra will be referred to as a microzone. Inside each microzone, this method assumes that the energy bands vary linearly, and thus the surface of constant energy is a plane.

Generating the nonoverlapping tetrahedral microzones is easy once it is realized that the irreducible wedge (1/48th) of the Brillouin zone is also tetrahedra,. Constructing the mid-points of $\Gamma \rightarrow$ P, $\Gamma \rightarrow$ N, $\Gamma \rightarrow$ H, N $\rightarrow$ H, N $\rightarrow$ P, P $\rightarrow$ H lines and joining them results in eight nonoverlapping tetrahedra. Each of these tetrahedra may be further subdivided into eight microzones that are octahedral and nonoverlapping, and so on. The total number thus obtained is 8^p where p is the cycle number.

Once the microzones are generated, it becomes convenient to arrange the energies at the corners of any of the tetrahedra in increasing or decreasing order. Let $\mathbf{k}_i$ $(i = 1\text{–}4)$ represent the coordinates of the *ith* corner of the tetrahedron. Denoting $E_n(\mathbf{k}_i)$ by E_i, the energies at the four corners can always be arranged such that

$$E_4 \leqq E_3 \leqq E_2 \leqq E_1; \tag{3}$$

and since the volume of each microzone can be made arbitrarily small it is then justifiable to express

$$E_i = E_4 + \mathbf{b} \cdot (\mathbf{k}_i - \mathbf{k}_4) \tag{4}$$

with

$$\mathbf{b} = \sum_{j=1}^{3} (E_i - E_4)\mathbf{r}_i$$

where

$$\mathbf{r}_i \cdot \mathbf{k}_j = \delta_{ij}$$

with

$$\mathbf{k}'_j = \mathbf{k}_j - \mathbf{k}_4, \quad j = 1\text{–}3$$

and

$$\mathbf{r}_1 = \frac{\mathbf{k}'_2 \times \mathbf{k}'_3}{6V};$$

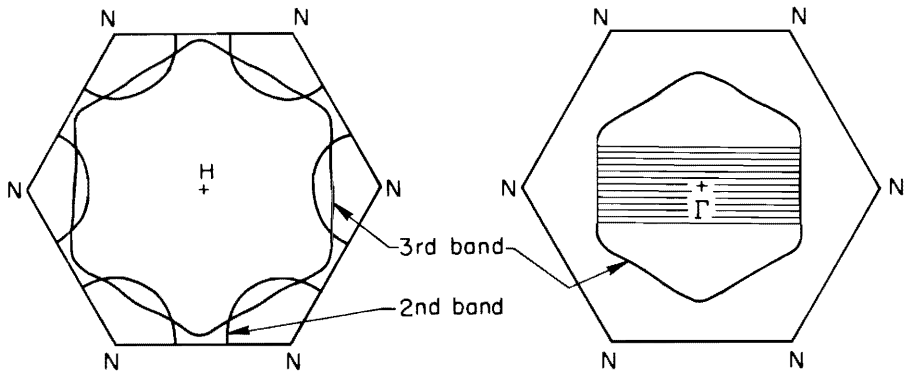

Figure 6. Fermi Surface Cross Sections in the (111) Plane

Table 3. Locations of the Intersections of the Fermi Surface with Zone Symmetry Lines. Lengths are Expressed in Units of $(2\pi/a)$.

Plane	Orbit	Direction	Length
		$\Gamma \rightarrow$ H	0.450
	Octagon about H	H → N	0.451
(100)			
	Ellipsoid about N	N → Γ	0.312
		N → H	0.182
	Dumbbell about P	P → N	0.385
		P → H	0.456
		P → Γ	0.456
(110)			
	Hole about Γ	Γ → N	0.396
		Γ → H	0.560
		Γ → P	0.406
(111)	Hole about Γ	Γ → N	0.409
		H → N	0.528
	Ellipsoid about N	H → N	0.421
		N → N	0.247

V is the volume of the tetrahedron. In this procedure the tetrahedra need not have the same volume; the only requirement is that the energy $E_n(\mathbf{k})$ within the microzone can be expanded linearly as required by the relation numbered (4).

Now the evaluation of the $\chi(\mathbf{q})$ boils down to (i) the calculation of the fractional volume of a given tetrahedron that contributes to the susceptibility function; and (ii) the evaluation of the contribution for a complete tetrahedron.

The fractional volume is that portion of the tetrahedron for which the Fermi factor $f(E_n(\mathbf{k}))\ [1 - f(E_m(\mathbf{k} + \mathbf{q}))]$ is equal to unity. After arranging the energies (Equation (3)), and making use of the planar constant energy surfaces assumption (Equation (4)), the fractional volume sought is the intersection of two regions. One of the regions is the one which is occupied by band $E_n(\mathbf{k})$, and the other corresponds to that region of the same tetrahedron which is unoccupied by band $E_m(\mathbf{k} + \mathbf{q})$. The n and m band indices may be identical. In the first region $f(E_n(\mathbf{k}))$ is equal to 1 and in the second $f(E_m(\mathbf{k} + \mathbf{q}))$ is equal to zero. For further details reference is made to the paper by Rath and Freeman [7].

The evaluation of the contribution for a complete microzone is effected by transforming the summation over $\mathbf{k}$ in expression (2) to an integral:

$$\chi(\mathbf{q}) = \frac{\Omega}{(2\pi)^3} \sum_{m,n} \int_{BZ} d^3k \frac{f(E_n(\mathbf{k}))\,[1 - f(E_m(\mathbf{k} + \mathbf{q}))]}{E_m(\mathbf{k} + \mathbf{q}) - E_n(\mathbf{k})} \quad (5)$$

where Ω is the volume of the Winger–Seitz cell. The contribution consists in evaluating the Fermi factor discussed earlier, and integrating

$$J_{nm}(\mathbf{q}) = \int_{\text{tetra}} \frac{d^3k}{E_m(\mathbf{k} + \mathbf{q}) - E_n(\mathbf{k})}. \quad (6)$$

Expanding the energy difference

$$E_m(\mathbf{k} + \mathbf{q}) - E_n(\mathbf{k}) = A + BX + CY + DZ,$$

the coefficients A, B, C, D are determined from the values of the energies at the corners of the tetrahedron, provided a linear expansion is assumed. Explicit expressions for J_{nm} for all possible cases are also given in reference [7].

Since the calculation of $\chi(\mathbf{q})$ requires the knowledge of $E_n(\mathbf{k})$ and $E_m(\mathbf{k} + \mathbf{q})$ at a very large number of points, fitting the calculated energy bands to an analytical expression is very desirable. The original band-structure is calculated for 140 points on the irreducible wedge. These are adequate for $\mathbf{k}$ but very restrictive to the values of $\mathbf{q}$ that can be used to calculate $E_m(\mathbf{k} + \mathbf{q})$. This is restrictive in the sense that we might be unable

to select those values of $\mathbf{q}$ at which the structure in the susceptibility might occur.

The periodicity of the bandstructure, $E_n(\mathbf{k}) = E_n(\mathbf{k} + \mathbf{K}_s)$ ($\mathbf{K}_s$ is a reciprocal lattice vector), suggests the following form for the analytical fit

$$E_n(\mathbf{k}) = \sum_{\mu} a_n(\mathbf{R}_\mu)\exp(i\mathbf{k} \cdot \mathbf{R}_\mu), \qquad (7)$$

where $\mathbf{R}_\mu$ is a direct lattice vector, and the a_n are the coefficients to be determined for the band n. Computational details of this, and of the evaluation of Equation (5) are given in the following section.

4. SUSCEPTIBILITY RESULTS

In the evaluation of the susceptibility, the analytical fit suggested in Equation (7) was transformed into an eigenvalue equation of the following form:

$$\sum_{\nu} \{E_n(\mathbf{k}) - \sum_{\mu} a_n(\mathbf{R}_\mu) \exp(i\mathbf{k} \cdot \mathbf{R}_\nu)\} \exp(-i\mathbf{k} \cdot \mathbf{R}_\nu) = 0$$

The summations over the indices ν and μ were carried out over 35, 52, and 65 closed shells of the direct lattice. The root mean square fit for the bands under consideration improved by 1 part in 10^4 in going from 52 to 65. The summation over the band under n (m) was carried out for six bands.

To evaluate the integral over $\mathbf{k}$, the irreducible wedge (1/48th of the Brillouin zone) was divided into 512 microzones. Calculation of Equation (5) for 3 different values of $\mathbf{q}$ with 4096 microzones yielded a change ($\sim 10^{-4}$) in the $\chi(\mathbf{q})$ value with 512 microzones. That did not justify the computer time expenditure. For all the results reported here, the evaluation of Equation (5) utilized 512 microzones. On the other hand, a calculation with 64 microzones resulted in a change of about 8% of $\chi(\mathbf{q})$. These results reflect on the validity of the linearity assumption (Equation (4)) of the energy bands within a microzone.

Plots of $\chi(\mathbf{q})$ along the three crystallographic directions [100], [110], and [111] are shown in Figures 7, 8 and 9, respectively. In the [100] three distinct peaks occur, at $|\mathbf{q}|$ values of 0.453, 0.550, and 0.750. The $|\mathbf{q}|$ values given here are in units of $(2\pi/a)$. For the first two peaks the value of the susceptibility is 120% $\chi(\mathbf{q} = 0)$. $\chi(\mathbf{q} = 0)$ is equal to the density of states at E_F. The $\chi(\mathbf{q})$ in the [110] is symmetric about the value $\mathbf{q} = 0.500$ (units of $\sqrt{2}\,\pi/a$). The structures occur at $\mathbf{q} = 0.455$ and 0.540, in the same units. The value of the susceptibility at the two structures is 125% $\chi(\mathbf{q} = 0)$.

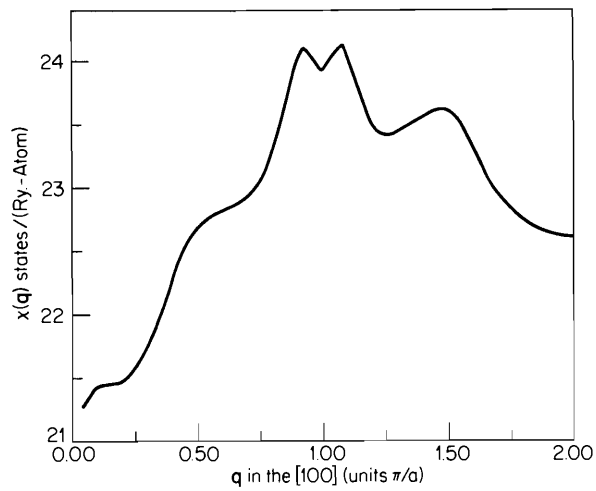

Figure 7. Bare Susceptibility in the [100] Direction

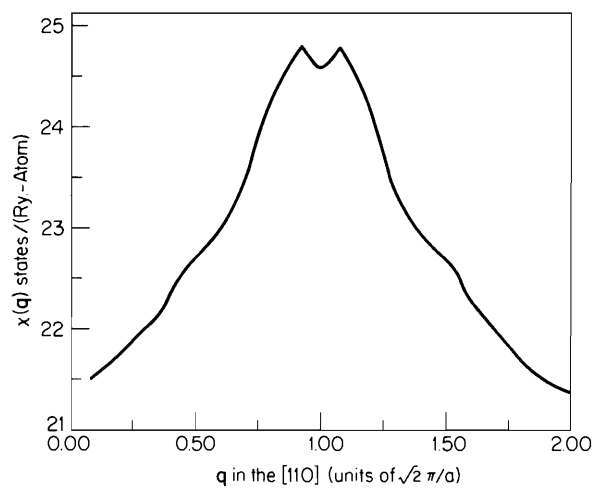

Figure 8. Bare Susceptibility in the [110] Direction

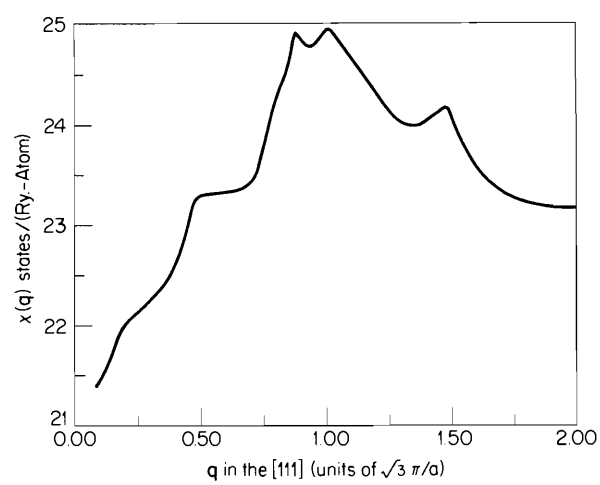

Figure 9. Bare Susceptibility in the [111] Direction

Structures in the [111] occur at relatively the same $|\mathbf{q}|$ values as in the [100].

Based on the observations that the $\chi(\mathbf{q})$ in the [110] does not exhibit any structure at a $|\mathbf{q}|$ value of 0.75, and that the electron surface dumbbell about N does not intersect the (110) plane; it is suggested here that the structure at $|\mathbf{q}| = 0.75$ results from a nesting of the dumbbell with portions of the octahedral surface about H. The dimensions of the dumbbell are too small to support nesting at such a 'large' value of $\mathbf{q}$. The pair of structures centered at $|\mathbf{q}| = 0.50$ result from the nesting of the same surface: the electron hole about Γ. A possible nesting which may account for the structure at $|\mathbf{q}| = 0.455$ is suggested in Figure 6. For the structure at $|\mathbf{q}| = 0.540$, the shaded area in Figure 5 is suggested as a possible nesting situation.

The above results have been obtained from a calculation for which the matrix elements $M_{n,m}$ in Equation (2) were taken to be constant. It is an accepted fact [28], that in the calculations that included the matrix elements [21] the structures in the $\chi(\mathbf{q})$ that result from the nesting of the same surface are slightly modified. The effect of including the matrix elements is prominant (tends to smoothen the effect) in the case of nesting between two distinct surfaces. Based on this observation, it is believed that the structure at $|\mathbf{q}| = 0.75$ may disappear in a calculation that includes matrix elements contributions. The two structures resulting from the hole surface will remain relatively unaffected [29].

In order to relate the structure of $\chi(\mathbf{q})$ to the possible occurrence of an instability, the structure has to be related to the phonon dispersion curves. It is generally believed that the kinks in the phonon curves arise from peaks in $\chi(\mathbf{q})$ [11], and that the diagonal element of the dielectric function $\epsilon(\mathbf{q}, \mathbf{q})$ is related to $\chi(\mathbf{q})$ through the relation [7]

$$\epsilon(\mathbf{q}, \mathbf{q}) = 1 + A\, I(\mathbf{q})\, \chi(\mathbf{q}),$$

where A is a constant, and $I(\mathbf{q})$ is the transform of the electrostatic electron–electron interaction including exchange and correlation effects. Since the dielectric screening by the conduction electrons plays an important role in determining the ion–ion interaction transmitted by the conduction electrons, one might expect a sharp maximum in $\chi(\mathbf{q})$ to manifest itself also as a Kohn anomaly in the phonon dispersion curve [30]. The occurrence of this anomaly is marked by the existence of a phonon soft mode which is responsible for a peak in the $I(\mathbf{q})$ occurring in Equation (1). Recently Moss *et al.* [31] have cast this mechanism in phonon language indicating how a body-centered cubic → hexagonal close packed transformation can be accomplished through the combined action of a soft long wavelength [112] Shear mode, polarized in [111], followed by a zone boundary [110] shear, polarized in [110]. To characterize the softening of this mode, Moss [32] performed inelastic neutron studies on several alloys of low solute concentration in which it was clear that the dynamical response of the body-centered cubic lattice was extremely anomalous, including very overdamped phonons and a central quasi-elastic peak, especially in the vicinity of $\frac{2}{3}$[111].

The phonon frequencies around $\frac{2}{3}$[111] in body-centered cubic lattices are naturally soft. Price *et al.* [33] showed, if the separate eigenvalue contributions to the dynamical matrix are represented by Coulombic (arising from BCC lattice + Ze charges immersed in a neutralizing electron gas), electron–ion (the effect of screening) and core-repulsive parts, then the unscreened Coulombic part alone gives rise to a deep dip near the $\frac{2}{3}$[111] for longitudinal modes. Normal screening merely pulls the small $\mathbf{q}$ low-frequency modes down toward zero to give the proper acoustic velocity. For this reason metals as dissimilar as Na, β-Cu, Zn, Fe, and Nb show pronounced minima in the longitudinal phonon dispersion curve at $\mathbf{q} = \frac{2}{3}$[111].

Further, the problem of the soft phonon mode leading to periodic lattice distortion as a consequence of nesting Fermi surfaces has been considered by Chan and Heine [11]. To investigate how the electron–phonon interaction renormalizes the phonon frequency, the authors supposed that the lattice system is driven into a single phonon mode $\mathbf{q}$. The electron–phonon coupling scatters electrons from state $\mathbf{k}$ to state $\mathbf{k} + \mathbf{q}, \mathbf{k} + \mathbf{q} + \mathbf{K}_s$ ($\mathbf{K}_s$ is a reciprocal lattice vector). This way, the movement of the electrons screens the phonon mode. The screening depends on the geometry of the Fermi surface. If the geometry is such that $\mathbf{q}$ approximately spans two nesting pieces of Fermi surfaces, and if the electron–phonon coupling is strong enough, the phonon mode may become soft. Lattice distortion thus takes place and the phonon frequency may be reduced to show a cusp shaped Kohn anomaly in the phonon spectrum. The scattering of the electrons by this phonon mode sets up a charge density wave of wave vector $\mathbf{q}$.

In our investigation, the calculated density of states curve determined from the reported bandstructure exhibits a large DOS at the Fermi level. This DOS is equal to 21.18 states (Ry-atom) which is approximately twice that of Fe [27], and will result in a large electron–phonon term for the metal under consideration. The

susceptibility exhibits two peaks that result from the nesting of the electron-hole about Γ. And, by the arguments presented above, this structure coupled to the naturally occurring BCC soft longitudinal phonon mode are sufficient conditions for the occurrence of an instability that transforms the β-Ti crystal to the α phase. This instability is of the periodic lattice distortion coupled to a charge density wave type. The investigation of the β-Ti at low solute concentration taking into account the effects of lattice contractions are underway and will be the subject of a future communication.

ACKNOWLEDGMENT

The author is grateful to Dr. J. Rath for many helpful conversations concerning this investigation, and for his generosity in making his code available to the author. Special thanks are due to Dr. T. J. Greene for a careful reading of the manuscript and for helpful comments.

REFERENCES

[1] R. A. Tawil and S. P. Singhal, *Physical Review*, **B11** (1975), p. 699.
[2] S. P. Singhal, *Physical Review*, **B12** (1975), p. 564; **B12** (1975), p. 6007.
[3] R. A. Tawil, *Physical Review*, **B11** (1975), p. 4891.
[4] L. F. Mattheiss, *Physical Review*, **B3** (1973), p. 3719.
[5] D. G. Laurent, C. S. Wang and J. Callaway, *Physical Review*, **B17** (1978), p. 4550.
[6] A review of the extensive work accumulated is beyond the scope of this paper; the papers numbered [1–5] and the references therein are suggested.
[7] J. Rath and A. J. Freeman, *Physical Review*, **B11** (1975), p. 2109.
[8] A. J. Freeman, H. W. Myron, J. Rath and R. P. Gupta, *International Journal of Quantum Chemistry, Symposium No. 9* (1975), p. 535.
[9] O. Gunnarsson, *Journal of Physics*, **C5** (1976), p. 587.
[10] T. Izuyama, D. J. Kim and R. Kubo, *Journal of Physical Society of Japan*, **18** (1963), p. 1025.
[11] S. K. Chan and V. Heine, *Journal of Physics*, **F3** (1973), p. 795.
[12] R. M. Welch and E. H. Hygh, *Physical Review*, **B9** (1974), p. 1993.
[13] O. Jepsen, O. K. Andersen and A. R. Mackintosh, *Physical Review*, **B12** (1975), p. 3084.
[14] S. L. Altmann and C. J. Bradley, *Proceedings of the Physical Society*, **92** (1967), p. 764.
[15] G. N. Kamm and J. R. Anderson, *Low Temperature Physics*. **Vol. 4**, New York, Plenum, 1974.
[16] P. M. Everett, *Physical Review*, **B6** (1972), p. 3559.
[17] O. Jepsen, *Physical Review*, **B12** (1975), p. 2988.
[18] W. B. Pearson, *Handbook of Lattice Parameters*. New York, Perganon Press, 1958, p. 876.
[19] Reference [18] p. 872; and references therein that explain the symbols in Figure 1.
[20] A. W. Overhauser, *Journal of Applied Physics*, **34** (1963), p. 1019; and references therein.
[21] S. Liu, R. P. Gupta and S. K. Sinta, *Physical Review*, **B4** (1971), p. 1100.
[22] J. F. Cooke, H. L. Davis and M. Mostoller, *Physical Review*, **B9** (1974), p. 2485.
[23] R. A. Tawil and T. J. Greene, *Arabian Journal for Science and Engineering*, **2** (1977), p. 113.
[24] R. Gaspar, *Acta Physica Academic Science of Hungary*, **3** (1954), p. 263; W. Kohn and L. J. Sham, *Physical Review*, **140** (1965), p. A1133.
[25] A. J. H. Wachters, *Journal of Chemical Physics*, **52** (1970), p. 1033.
[26] E. C. Snow and J. T. Waber, *Acta Metallurgica*, **17** (1969), p. 623.
[27] R. A. Tawil and J. Callaway, *Physical Review*, **B7** (1973), p. 4242.
[28] J. Rath, Private Communication.
[29] R. P. Gupta, J. Rath and A. J. Freeman (to be published).
[30] W. Kohn, *Physical Review Letters*, **2** (1959), p. 393.
[31] S. C. Moss, D. T. Keating and J. D. Axe, *Solid State Communication* **13** (1973), p. 1465.
[32] J. D. Axe, D. T. Keating and S. C. Moss, *Bulletin of the American Physical Society*, **19** (1974), p. 321.
[33] D. L. Price, K. S. Singwi and M. P. Tosi, *Physical Review*, **B2** (1970), p. 2933.

Paper Received 1 May 1978.